Jurnal Teknologi

Full Paper

REFORMULATED STRAIN GRADIENT (RSG) ELASTICITY THEORY FOR FREE VIBRATION OF THERMAL BI-DIRECTIONAL FG MICROBEAM

Safa Hameed Majeed, Talib Ehraize Elaikh*, Adnan Abdul-hussien Ugla

Department of Mechanical Engineering, College of Engineering, University of Thi-Qar, Thi-Qar,64001, Iraq

Article history
Received
23 August 2023
Received in revised form
9 October 2023
Accepted
9 October 2023
Published Online
18 February 2024

*Corresponding author
talib-h@utq.edu.iq

Graphical abstract

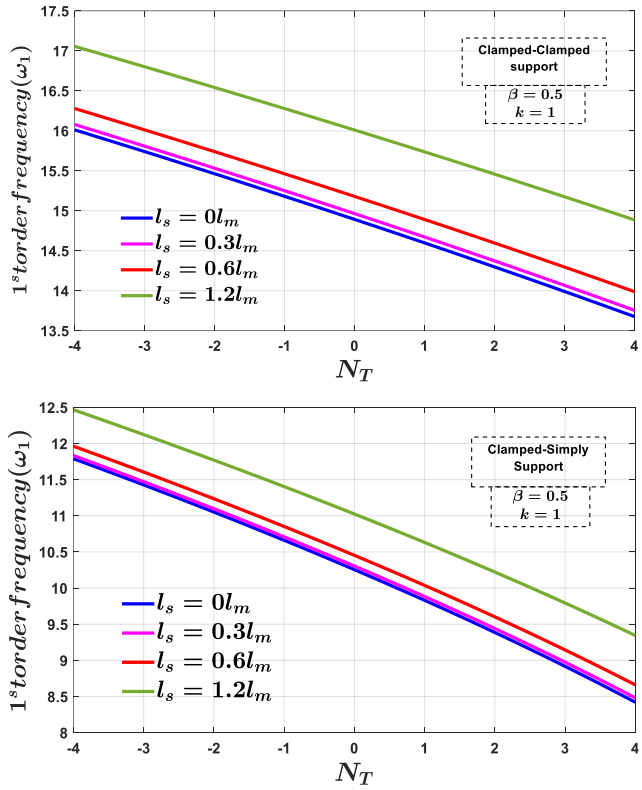

Abstract

This research examines the vibrational response of a micro-scale Euler beam made from two-directional functionally graded (2D-FG) materials and subjected to thermal effects. By employing a reformulated strain gradient elasticity (RSGE) approach, the equations of motion using Hamilton's principle for clamped -clamped and clamped-simply boundary conditions are derived and solved them using Galerkin's approach. The investigation explores the impact of temperature, gradient index, and parameters length scale materials on the bidirectional graded microbeam's dynamic characteristics. Furthermore, the normalized frequency, as based on the current reformulated strain gradient elasticity microbeam model, consistently emerges as higher than that derived from the classical model.

Keywords: Bidirectional FGM microbeam, RSGE, Galerkin method (GM), thermal effect

1.0 INTRODUCTION

Functionally graded materials (FGMs), which possess highly effective mechanical and thermal properties, have received significant attention recently for use in many engineering applications, such as in aircraft, spacecraft, defense industries, electronics, and biomedical fields. [1], [2]. FGM can be created using a variety of material combinations, the most popular being metal-metal, metal-ceramic, ceramic-ceramic, or ceramic-polymer [3]. Properties of FGM are varied either in one direction [4] (i.e., thickness or

longitudinal) or bi-direction (in both thickness and longitudinal)[5].

Moreover, many microelectromechanical systems (MEMS) predominantly consist of continuous microstructures like microbeams, microplates, micro pipe [6], and micro arches [7]. Functionally graded nano/microscale structures represent an advanced category of small-scale systems with promising applications in both nano- and microtechnology [8], [9].

Indeed, certain studies have assumed that graded materials exhibit property gradients in two distinct directions. For instance, Şimşek [10]considered a graded Euler-Bernoulli beam where material properties vary along both axial and thickness directions, following a power law. Their findings reveal that, unlike homogeneous beams, 2D-FG beams display discernible buckling mode shapes. Moreover, shear effects exhibit heightened sensitivity in the behavior of double-clamped beam ends when compared to other types of beams. Avcar [11] formulated the motion equation for beams with varying end conditions, encompassing simply-supported, clamped-pinned, fixed-fixed, and cantilever setups. This formulation was based on the Euler model and solved using the Newton-Raphson method. The outcomes of this study highlighted that the first three modes were influenced by both the geometric characteristics and the specific end conditions in play. Karamanli et al. [12] analyzed the impact of variable Material Length Scale Parameters (MLSP) on the dynamic behavior of 2D FG porous microbeams. The outcomes of their study revealed that incorporating variable MLSP resulted in increased frequencies and buckling loads, accompanied by decreased displacements.

The classical continuum theory often overlooks size effects, leading to inaccurate predictions for the behavior of micro/nano-structures [13]. Consequently, when studying the vibrational behaviors of small-sized FG nano/micro beams, non-classical theories such as MCST and MSGT were employed [14]. Based on modified couple stress (MCS) and shear deformable beam theories, [15] analyzed the nonlinear vibration of imperfect BDFG microbeams and found that increasing the length scale parameter results in a decrease in the nonlinear frequency ratio. Lam et al., [16] were pioneers in introducing the modified strain gradient theory (MSGT) as an advanced higher-order continuum theory.

Akgöz and Civalek [17] investigated the buckling behavior of FG microbeams and concluded that the variance between the non-dimensional critical buckling loads obtained by MSGT, MCST, and classical continuity models gradually decreased because of the rise in the material length-to-thickness scale parameters. Ansari et al., [18] conducted an investigation into the free vibration behavior of micro-sized beams. Their findings revealed that the natural frequencies obtained using the modified strain gradient theory (MSGT) were both higher and more accurate compared to the results obtained through the modified couple stress theory (MCST) as well as the classical theory (CT). The gradient index exhibits a slightly lesser influence on the dynamic behavior in the thickness direction compared to its effect in the length direction, as observed by Ref. [19].

Recently, static bending and free vibration of microbeams were investigated by [20], utilizing reformulated microbeam models and the general strain gradient elasticity theory (GSGET). This study revealed that microbeams based on non-classical theories, particularly GSGET, exhibit greater stiffness than models based on classical theory. Based on (RSGET), the vibration governing equations for Timoshenko–Ehrenfest beam were acquired by [21]. The proposed analytical solution revealed a reduced deflection and a higher natural frequency in the non-classical model utilized. In Ref. [22], static and dynamic aspects of FG Bernoulli-Euler micro-size beams were conducted. The study concluded that the FG microbeam fundamental frequency based on (RSGT) was greater compared to that of (MCST). Yin et al., [23] introduced analytical solutions for post-buckling size-dependent EBT and TBT microbeams and examined the impact of beam thickness and other parameters on the post-buckling response. Yin et al., [24] examined the buckling behavior of size-dependent microbeams using both exact solutions and the isogeometric analysis method. The study revealed significant variations in the critical buckling load obtained from RSGET, MCST, and classical theory as the length-to-thickness ratio (L/h) decreased, and these variations increased as the strain gradient length–scale parameter (l_s) increased. Yin et al. [25] introduced IGA for targeting micro-size Euler-Bernoulli beams, utilizing the (RSGT). They demonstrated the effectiveness of their approach by conducting a comparative analysis between their numerical results and established analytical solutions. Zhang and Gao [26] introduced the concept of the (RSGT) to study the free vibration of double simply Bernoulli beam. The authors incorporated three distinct material length scale parameters, providing a comprehensive framework to better understand the collaborative behavior of this modified new theory.

On the other hand, the effect of temperature changes on the dynamic performance of structures made of functionally graded (FG) materials was investigated. In this regard, many studies have been conducted to explore the thermal and mechanical effects on the dynamic behavior of these structures[27]. Zanoosi [28] studied the effect of the thermal environment on the vibration response of porous (FG) microbeams considering (MSGT). Hamilton's principle was acquired to get the simply supported beam governing equation and Navier's solution was employed to obtain the system's natural frequency. Tang and Ding [29] studied the hygro-thermal nonlinear vibration of the bi-directional FG beam. Hamilton's principal and geometric nonlinearity with Bernoulli-Euler was employed to find

the governing equation. Their investigation revealed a significant finding: as the bi-directional FG indexes increased, the nonlinear frequency exhibited a decrease. In contrast, the nonlinear frequency increased with higher vibration amplitudes. Utilizing the Modified Couple Stress Theory (MCST), [30] conducted an analysis of the thermal behavior exhibited by Functionally Graded (FG) microbeams. Their findings indicated that the impact of thermal effects was more pronounced in cases where the microbeams had higher values of the slenderness ratio (h/l) ratio. In Ref. [31] , the finite element (FE) method was utilized to analyze the response of a 2D-FG beam under the influence of a moving load. Their research integrated the Modified Couple Stress Theory (MCST) and Hamilton's principle to formulate the governing equations for the system. In Ref. [32], a study was conducted that focused on investigating the impact of end beam conditions on the thermal buckling load of a two-dimensional Functionally Graded (2D FG) beam. The researchers observed that the temperature-critical buckling for the Clamped-Clamped beam configuration was higher compared to the Hinged-Hinged beam configuration. Additionally, they noted that the C-C beam exhibited the highest natural frequency in the pre-buckling zone, while the H-H beam showed the highest frequency in the post-buckling region. The Clamped-Hinged beam configuration displayed intermediate behavior across all temperature ranges.

On the other hand, the Galerkin method has been widely utilized by researchers due to its shorter computation time for disbanding governing equation for macro and micro structure [33]–[36].

This paper aims to analyze the thermal vibrational behavior of two-directional functionally gradient non-classical (FG) microbeams based on the reformulated strain gradient elasticity (RSGE) approach. The governing equations of motion are derived using Hamilton's principle with the two end conditions (i.e., C-C and C-S). The resulting equations are solved using the Galerkin method, then the dimensional equations are converted to non-dimensional equations to obtain more comprehensive results. The obtained results from the 2D-FG microbeam are compared with the results of previous research. The effect of temperature, the material gradient index (k),the axial gradient index (β), and different material length scale parameters on non-dimensional natural frequencies of the 2D-FG RSGT microbeam model are discussed.

2.0 METHODOLOGY

The schematic diagram of (BDFG) microbeam is shown in Figure 1. The distance between the two supports is denoted as L, the cross-sectional width as b, and the thickness as h. The top and bottom beam surfaces are composed of ceramic and metal, respectively.

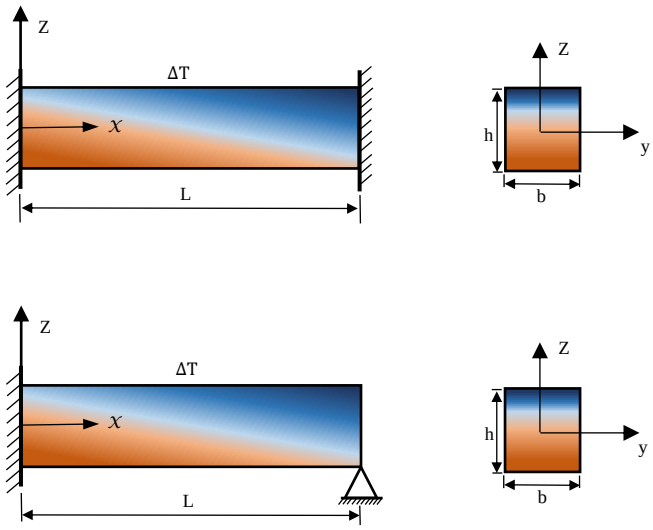

Figure 1 Scheme diagram of double-clamped and clamped-simply supported ends of 2D-FG microbeam and cross-sections

2.1 BDFG Microbeams Governing Equation

The material properties used in this work vary continuously in two directions. The effective modulus of elasticity $E(x,z)$, effective density $\rho(x,z)$, and effective thermal expansion $\alpha(x,z)$ coefficient in two-directions are given as follows [37]:

$$E(x,z) = f_1(x)E(z) = f_1(x)\left[(E_c - E_m)\left(\frac{z}{h}+\frac{1}{2}\right)^k + E_m\right] \quad (1)$$

$$\rho(x,z) = f_2(x)\rho(z) = f_2(x)\left[(\rho_c - \rho_m)\left(\frac{z}{h}+\frac{1}{2}\right)^k + \rho_m\right] \quad (2)$$

$$\alpha(x,z) = f_3(x)\alpha(z) = f_3(x)\left[(\alpha_c - \alpha_m)\left(\frac{z}{h}+\frac{1}{2}\right)^k + \alpha_m\right] \quad (3)$$

In the x direction, the material properties change according to the exponential function, as given by [5]:

$$f_1(x) = f_2(x) = f_3(x) = e^{\beta\frac{x}{L}} \quad (4)$$

where β represents the axial FG index, It should be noted that the characteristics of the mentioned material elements are not linear functions of temperature and can be described as follows [38]:

$$H = H_0(H_{-1}T^{-1} + 1 + H_1T + H_2T^2 + H_3T^3) \quad (5)$$

Here, as shown in Table 1, H_0, H_{-1}, H_1, H_2 *and* H_3 are the specific temperature (T, Kelvin) dependent material coefficients, where $T = T_0 + \Delta T$, $T_0 = 300K$. This work omitted the consideration of linear and non-linear temperature distributions [39].

Table 1 Si3N4 and SUS304 coefficients properties vary with temperature [39]

Material	Property	H_{-1}	H_0	H_1	H_2	H_3	H (T=300K)
Si_3N_4	$E(Pa)$	0	348.43e + 9	-3.070e-4	2.160e-7	-8.946e-11	3.2227e+11
	υ	0	0.24	0	0	0	0.24
	$\alpha(1K^{-1})$	0	5.8723e-6	9.095e-4	0	0	7.4746e-06
	$\rho(kg/m^3)$	0	2370	0	0	0	2370
$SUS304$	$E(Pa)$	0	201.04e+9	3.079e-4	-6.534e-7	0	207.7877e+9
	υ	0	0.3262	-2.002e-4	3.97e-7	0	0.3177
	$\alpha(1K^{-1})$	0	12.33e-6	8.086e-4	0	0	15.32e-6
	$\rho(kg/m^3)$	0	8166	0	0	0	8166

2.2 Kinematic Relation

This research adopts the (RSGET), which was first introduced by[26]. The advantage of this theory lies in its utilization of two scale parameters, one to capture the effect of couple stress and the other to account for the effect of strain gradient. The strain energy U based on the RSGET, considering an isotropic linear elastic body, is calculated as follows:

$$U = \frac{1}{2}\int_0^L \int_A \left(\sigma_{ij}\varepsilon_{ij} + \tau_{ijk}^s \eta_{ijk}^s + m_{ij}\chi_{ij}\right) dA dx \quad (6)$$

where the Cauchy stress tensor, σ_{ij}, the symmetric part of the double-stress tensor, τ_{ijk}^s, and the couple-stress tensor, m_{ij}, are given by

$$\sigma_{ij} = \lambda(x,z)\varepsilon_{kk}\delta_{ij} + 2\mu(x,z)\varepsilon_{ij} \quad (7)$$

$$\tau_{ijk}^s = 2l_s^2\mu(x,z)\eta_{ijk}^s \quad (8)$$

$$m_{ij} = 2l_m^2\mu(x,z)\chi_{ij} \quad (9)$$

where λ and μ are the Lamé parameters, the symbol δ_{ij} refers to the Kronecker delta. The quantities of ε_{ij}, η_{ijk}^s, θ_i , and, χ_{ij}, are, respectively, expressed by:

$$\varepsilon_{ij} = \frac{1}{2}\left(u_{i,j} + u_{j,i}\right) \quad (10)$$

$$\eta_{ijk}^s = \frac{1}{3}\left(u_{i,jk} + u_{j,ki} + u_{k,ij}\right) \quad (11)$$

$$\chi_{ij} = \frac{1}{2}\left(\theta_{i,j} + \theta_{j,i}\right), \quad \theta_i = \frac{1}{2}e_{ijk}u_{k,j} \quad (12)$$

The displacements of slender microbeams can be depicted using the Euler-Bernoulli theory as:

$$u_1 = -z\frac{\partial w(x)}{\partial x}\,,\ u_2 = 0,\ u_3 = w(x) \quad (13)$$

The strain component, gradient second-order, and curve vector are obtained by inserting displacement Equation (13) into Equations (10-12).

$$\varepsilon_{xx} = -z\frac{\partial^2 w}{\partial x^2},\ \eta_{xxx}^s = -z\frac{\partial^3 w}{\partial x^3}\,,\ \eta_{xxz}^s = -\frac{1}{3}\frac{\partial^2 w}{\partial x^2} \quad (14a)$$

$$\chi_{xy} = -\frac{1}{2}\frac{\partial^2 w}{\partial x^2}, \qquad \theta_y = -\frac{\partial w}{\partial x} \quad (14d)$$

As η_{xxx}^s is higher order than the displacement gradient η_{xxz}^s [40], [41]. Because of this, η_{xxx}^s effect is ignored throughout the formulation[24]

$$\sigma_{xx} = -E(x,z)z\frac{\partial^2 w}{\partial x^2} \quad (15a)$$

$$\tau_{xxz}^s = -\frac{2}{3}l_s^2\mu(x,z)\frac{\partial^2 w}{\partial x^2} = -\frac{1}{3}l_s^2\frac{E(x,z)}{(1+\upsilon)}\frac{\partial^2 w}{\partial x^2} \quad (15b)$$

$$m_{xy} = -\mu(x,z)l_m^2\frac{\partial^2 w}{\partial x^2} = -l_m^2\frac{E(x,z)}{2(1+\upsilon)}\frac{\partial^2 w}{\partial x^2} \quad (15c)$$

The strain energy of the BDFG microbeam, resulting from the strain and stress, can be obtained using Equations (14), (15), and (6):

$$U_S = \frac{1}{2}\int_0^L \left(f_1(x)EI_{eq}\left(\frac{\partial^2 w}{\partial x^2}\right)^2 + f_1(x)\frac{EA_{eq}}{2(1+\upsilon)}l_m^2\left(\frac{\partial^2 w}{\partial x^2}\right)^2 + \frac{1}{3}f_1(x)\frac{EA_{eq}}{(1+\upsilon)}l_s^2\left(\frac{\partial^2 w}{\partial x^2}\right)^2\right) dx \quad (16)$$

The kinetic energy of bi-directional FG microbeam is given as:

$$K_E = \frac{1}{2}\int_A \int_0^L \rho(x,z,t)\left(\frac{\partial w}{\partial t}\right)^2 dx dA = \int_0^L f_2(x)\,\rho A_{eq}\left(\frac{\partial w}{\partial t}\right)^2 dx \quad (17)$$

Due to the thermal load applied to the microbeam, the external work is expressed as follows:

$$W = \frac{1}{2}\int_0^L N_T\left(\frac{\partial w}{\partial x}\right)^2 dx,\ \ \delta W = \int_0^L (N_T)\left(\frac{\partial w}{\partial x}\right)\delta\left(\frac{\partial w}{\partial x}\right) dx \quad (18)$$

In the case of rising temperatures, N_T can be written as:

$$N_T = \int_A E(x,z,t)\,\alpha(x,z,t)\,\Delta T dA = \Delta T\, f_1(x)f_3(x)\bar{N}_T = \Delta T\, f_1(x)f_3(x)\ \ E_c\alpha_c A\gamma_2 \quad (19)$$

Hamilton's precept general form is given as:

$$\int_{t_1}^{t_2}(\delta K_E - \delta U_S + \delta W)dt = 0 \quad (20)$$

After inserting the expressions for strain energy (16), kinetic energy (17), and external work (18) into Hamilton's principal equation (20) and applying integration by parts, the dynamic equation of

bidirectional FG Euler microbeams is derived as follows.:

$$\left[El_{eq}+\frac{EA_{eq}}{2(1+\nu)}l_m^2+\frac{2}{3}\frac{EA_{eq}}{2(1+\nu)}l_s^2\right]\left(f_1(x)\left(\frac{\partial^4 w}{\partial x^4}\right)+2f_1'(x)\left(\frac{\partial^3 w}{\partial x^3}\right)+f_1''(x)\left(\frac{\partial^2 w}{\partial x^2}\right)\right)+\left[f_1(x)f_3(x)\,E_c\alpha_c A\gamma_2\Delta T\right]\left(\frac{\partial^2 w}{\partial x^2}\right)+\left[f_1(x)f_3'(x)+f_1'(x)f_3(x)\right]E_c\alpha_c A\gamma_2\Delta T\left(\frac{\partial w}{\partial x}\right)+f_2(x)\,\rho A_{eq}\frac{\partial^2 w}{\partial t^2}=0 \quad (21)$$

where,

$$EI_{eq}=b\int_{-\frac{h}{2}}^{\frac{h}{2}}E(z,t)z^2\,dz=b\int_{-\frac{h}{2}}^{\frac{h}{2}}\left[(E_c-E_m)\left(\frac{z}{h}+\frac{1}{2}\right)^k+E_m\right]z^2dz=E_cI\gamma \quad (22)$$

$$EA_{eq}=b\int_{-\frac{h}{2}}^{\frac{h}{2}}E(z,t)\,dz=b\int_{-\frac{h}{2}}^{\frac{h}{2}}\left[(E_c-E_m)\left(\frac{z}{h}+\frac{1}{2}\right)^k+E_m\right]dz=E_cA\alpha_1 \quad (23)$$

$$\rho A_{eq}=b\int_{-\frac{h}{2}}^{\frac{h}{2}}\rho(z,t)\,dz=b\int_{-\frac{h}{2}}^{\frac{h}{2}}\left[(\rho_c-\rho_m)\left(\frac{z}{h}+\frac{1}{2}\right)^k+\rho_m\right]dz=\rho_cA\alpha \quad (24)$$

Equation (4) is substituted into Equation (21), resulting in the following equation:

$$\left[EI_{eq}+\frac{E_cA\alpha_1}{2(1+\nu)}l_m^2+\frac{1}{3}\frac{E_cA\alpha_1}{(1+\nu)}l_s^2\right]e^{\frac{\beta}{L}x}\left(\left(\frac{\beta}{L}\right)^2\frac{\partial^2 w}{\partial x^2}+2\frac{\beta}{L}\frac{\partial^3 w}{\partial x^3}+\frac{\partial^4 w}{\partial x^4}\right)+\left(e^{\frac{\beta}{L}x}.\rho_cA\alpha\right)\frac{\partial^2 w}{\partial t^2}+\left(E_c\alpha_cA\gamma_2\Delta T.e^{\frac{\beta}{L}x}\right)\frac{\partial^2 w}{\partial x^2}+\left(2\frac{\beta}{L}e^{2\frac{\beta}{L}x}.E_c\alpha_cA\gamma_2\Delta T\right)\frac{\partial w}{\partial x}=0 \quad (25)$$

If $l_s=0$, then the MCST dynamic equation for the thermally loaded FG microbeam is as follows:

$$\left[E_CI\gamma+\frac{E_CA\alpha_1l^2}{2(1+\nu)}\right].e^{\frac{\beta}{L}x}\left[\left(\frac{\beta}{L}\right)^2\left(\frac{\partial^2 w}{\partial x^2}\right)+2\left(\frac{\beta}{L}\right)\left(\frac{\partial^3 w}{\partial x^3}\right)+\left(\frac{\partial^4 w}{\partial x^4}\right)\right]+\left[e^{2\frac{\beta}{L}x}.\alpha_CA\gamma_2\Delta T\right]\left(\frac{\partial^2 w}{\partial x^2}\right)+\left[2\left(\frac{\beta}{L}\right)e^{2\frac{\beta}{L}x}.\alpha_CA\gamma_2\Delta T\right]\left(\frac{\partial w}{\partial x}\right)+\left[e^{\frac{\beta}{L}x}.\rho_CA\alpha\right]\left(\frac{\partial^2 w}{\partial t^2}\right)=0 \quad (26)$$

When $l_s=0$ and $\beta=0$, the thermal vibration equation of the MCST FG microbeam is obtained, similar to the equation presented in Ref. [27].

For the 2D FG beam double-clamped and clamped-simply supported at both ends, the boundary condition equation is written as:

- Clamped-Clamped (C-C)

$$\left.\begin{aligned}w(0,t)=\frac{\partial w(0,t)}{\partial x}=0, &\quad at\ \ x=0\\ w(L,t)=\frac{\partial w(L,t)}{\partial x}=0, &\quad \text{at}\ \ x=L\end{aligned}\right\} \quad (27\text{-a})$$

- Clamped- Simply (C-S)

$$\left.\begin{aligned}w(0,t)=\frac{\partial w(0,t)}{\partial x}=0, &\quad at\ \ x=0\\ w(L,t)=\frac{\partial^2 w(L,t)}{\partial x^2}=0, &\quad \text{at}\ \ x=L\end{aligned}\right\} \quad (27\text{-b})$$

Dimensionless quantities are introduced as follows:

$$\xi=\frac{x}{L};\quad \eta=\frac{w}{L};\quad \tau=t.\sqrt{L^4\cdot\frac{\rho_c A}{E_c I}};\ N_T^{\sim}=\frac{E_c\alpha_cA\Delta TL^2}{E_cI} \quad (28)$$

A dimensionless equation of motion can be derived by substituting equation (28) into equation (25)

$$\left[\gamma+\frac{6\alpha_1}{(1+\nu)h^2}l_m^2+\frac{4\alpha_1}{(1+\nu)h^2}l_s^2\right]e^{\beta\xi}\left(\beta^2\frac{\partial^2\eta}{\partial\xi^2}+2\beta\frac{\partial^3\eta}{\partial\xi^3}+\frac{\partial^4\eta}{\partial\xi^4}\right)+\left(\gamma_2N_T^{\sim}.e^{2\beta\xi}\right)\frac{\partial^2\eta}{\partial\xi^2}+\left(2\beta N_T^{\sim}\gamma_2.e^{2\beta\xi}\right)\frac{\partial\eta}{\partial\xi}+\left(\alpha.e^{\beta\xi}\right)\frac{\partial^2\eta}{\partial\tau^2}=0 \quad (29)$$

Substituting equation (28) into equations (27), the dimensionless form of a clamped-clamped (CC) and clamped-simply (CS) boundary conditions can be expressed as:

$$\eta(0,\tau)=\eta(1,\tau)=0,\quad \frac{\partial\eta(0,\tau)}{\partial\xi}=\frac{\partial\eta(1,\tau)}{\partial\xi}=0 \quad (30\text{-a})$$

and,

$$\eta(0,\tau)=\eta(1,\tau)=0,\quad \frac{\partial\eta(0,\tau)}{\partial\xi}=\frac{\partial^2\eta(1,\tau)}{\partial\xi^2}=0 \quad (30\text{-b})$$

2.3 Solution Method

For discretizing the dynamic motion of a microbeam, the extended Galerkin is employed. The Galerkin technique involves selecting suitable weighting functions, represented as η, that fulfill the prescribed essential boundary conditions. These weighting functions are carefully chosen to ensure an accurate approximation of the transverse normalized displacement, denoted as η, using a series representation [35]:

$$\eta(\xi,T)=\sum_{r=1}^{n}\varphi_r(\xi)q_r(T) \quad (31)$$

where $\varphi_r(\xi)$ and $q_r(T)$ represents the shape function and generalized coordinates, respectively.

The mode shape $\boldsymbol{\varphi_r(x)}$ standards and the frequency equation of C-C are [42]:

$$\boldsymbol{\varphi_r(x)}=cosh(b_n\,x)-cos(b_n\,x)-\left(\frac{cosh\,(b_nL)-cos(b_nL)}{sinh\,(b_nL)-sin(b_nL)}\right)(sinh\,b_n\,x-sin\,b_n\,x) \quad (32)$$

$$cos\,b_n\,L\,cosh\,b_n\,L=1\ ;$$

$$where$$

$$b_1=4.730, b_2=7.853, b_3=10.996, b_4=14.137 \quad (33)$$

and for C-S boundary conditions are given as follows [42]:

$$\boldsymbol{\varphi_r(x)}=cosh(b_n\,x)-cos(b_n\,x)-\left(\frac{cosh\,(b_nL)-cos(b_nL)}{sinh\,(b_nL)-sin(b_nL)}\right)(sinh\,b_n\,x-sin\,b_n\,x) \quad (34)$$

$$\tan b_nL-\tanh b_nL=0;$$

$$where\ b_1=3.926, b_2=7.068, b_3=10.210, b_4=13.351 \quad (35)$$

By substituting equations mode shape (32) into equation (31), multiplying these equations by the residual function $\varphi_s(\xi)$, and integrating the resulting

equations from ξ=0 to ξ=1, the system equation is obtained as follows [33]

$$[M]\{\ddot{q}_r\} + [K]\{q_r\} = 0, \quad q_r = (q_r)^T \tag{36}$$

The microbeam stiffness [K] and mass [M] matrices equation are as follows [33]:

$$[M] = \alpha \int_0^1 e^{\beta\xi}\, \varphi_r \varphi_s d\xi \tag{37-a}$$

$$[K] = A\beta^2 \int_0^1 e^{\beta\xi}\, \varphi_r{}'' \varphi_s d\xi + 2A\beta \int_0^1 e^{\beta\xi}\, \varphi_r{}''' \varphi_s d\xi + A \int_0^1 e^{\beta\xi}\, \varphi_r{}^{IV} \varphi_s d\xi + \gamma_2 N_T^{\sim} \int_0^1 e^{2\beta\xi}\, \varphi_r{}'' \varphi_s d\xi 2\beta\gamma_2 N_T^{\sim} \int_0^1 e^{2\beta\xi}\, \varphi_r{}' \varphi_s d\xi \tag{37-b}$$

$$in\ which; A = \gamma + \frac{6\alpha_1}{(1+\nu)h^2} l_m^2 + \frac{4\alpha_1}{(1+\nu)h^2} l_s^2$$

It is possible to minimize the 2nd order differential equation (37) to a first-degree differential equation as follows [33]:

$$D\dot{Z}(T) + BZ(T) = 0 \tag{38}$$

$$\text{where, } D = \begin{bmatrix} M & 0 \\ 0 & 0 \end{bmatrix}, B = \begin{bmatrix} -M & 0 \\ 0 & K \end{bmatrix}, Z(T) = \begin{bmatrix} q(T) \\ \dot{q}(T) \end{bmatrix} \tag{39}$$

Given $Z(T) = Qe^{i\omega T}$, the eigenvalue problem is as follows:

$$YQ - i\omega J = 0 \tag{40}$$

where J represents the identity matrix, and $Y = -D^{-1}B$. Furthermore, ω denotes the natural frequency of 2-D FG microbeams.

3.0 RESULTS AND DISCUSSIONS

The BDFG-microbeam used in this work comprises Silicon Nitride Si3N4 (ceramics) and Stainless Steel SUS304 (metal) materials, where $k = 0$, and $k = \infty$, respectively. The geometric dimensions used in the numerical results are as follows: the beam width ($b = 2h$), the beam thickness $h = 5l$, and the beam length $L = 20h$. The couple stress length parameter is ($l = 17.6\mu m$)[25]. Poisson's ratio is a constant value of $\nu = 0.24$.

Galerkin's findings presented in this paper are validated by comparing them with the results of a Ref. [43] for an axial functionally graded (FG) microbeam under double-clamped (C-C) and clamped-simply supported (C-SS) composed of ceramic and metal with material properties as follows: $E = 210$ GPa, $\rho = 7800$ kg\$m^3$ for metal (SUS304), and $E = 390$ GPa, $\rho = 3960$ kg\$m^3$ for ceramic (Al2O3), by using MCST, as shown in Tables 2, 3. With an increase in the value of the material gradient index k, a decrease in the values of the non-dimensional natural frequencies was observed. The values of the fundamental frequencies in C-C case were higher than the C-SS condition, and this is due to the higher stiffness in the C-C. Additionally, a very close convergence was found between the results obtained.

Table 2 Comparison of the dimensionless natural frequency for C-C FG-microbeams

Frequency NO.	$\mathbf{L/h = 20}$, $\boldsymbol{\beta = 0}$, and $\boldsymbol{l/h = 0}$							
	$\boldsymbol{k = 0}$		$\boldsymbol{k = 0.2}$		$\boldsymbol{k = 1}$		$\boldsymbol{k = 10}$	
	Present	ref. [43]	Present	ref. [43]	Present	ref. [43]	Present	ref. [43]
$\boldsymbol{\omega_1}$	22.3733	22.3744	19.7545	19.7122	16.1034	15.8612	12.9342	12.8698
$\boldsymbol{\omega_2}$	61.6728	61.6847	54.4539	54.3455	44.3896	43.7292	35.6537	35.4811
$\boldsymbol{\omega_3}$	120.9034	120.9534	106.7515	106.5638	87.0213	85.7485	69.8955	69.5725
$\boldsymbol{\omega_4}$	199.8594	200.0034	176.4657	176.2120	143.8507	141.7957	115.5408	115.0417

Table 3 Present results comparison for (C-S) FG microbeams dimensionless frequency

Frequency NO.	$\mathbf{L/h = 20}$, $\boldsymbol{\beta = 0}$, and $\boldsymbol{l/h = 0}$							
	$\boldsymbol{k = 0}$		$\boldsymbol{k = 0.2}$		$\boldsymbol{k = 1}$		$\boldsymbol{k = 10}$	
	Present	ref. [43]	Present	ref. [43]	Present	ref. [43]	Present	ref. [43]
$\boldsymbol{\omega_1}$	15.4182	15.4189	13.6135	13.5884	11.0974	10.9534	8.9134	8.8751
$\boldsymbol{\omega_2}$	49.9649	49.9738	44.1164	44.0317	35.9627	35.4482	28.8852	28.7506
$\boldsymbol{\omega_3}$	104.2477	104.2887	92.0454	91.8850	75.0332	73.9537	60.2666	59.9922
$\boldsymbol{\omega_4}$	178.2697	178.3930	157.4031	157.1750	128.3113	126.4905	103.0595	102.6157

3.1 Influence of Gradient Index (k)

This subsection illustrates the impact of the power-law exponent and axial index on the natural frequencies of supported bidirectional functionally graded microbeams (BFGM), both with and without thermal effects. Figure 2 illustrates the variation in the fundamental frequency based on the classical theory (CT), (MCST), and (RSGET) for supported beams with varying thickness gradient indices. The results predicted by the classical theory can be derived from RSGET by setting $l_m = 0$ and $l_s = 0$, while MCST results can be obtained by setting $l_s = 0$. The material-scale parameter of RSGET in this calculation is assumed to be $l_s = 0.3\, l_m$.

As depicted in the Figure 2, the dimensionless first frequency predicted by RSGET and MCST consistently surpasses that obtained from the classical model. This observation also explains the size-dependent behavior. Furthermore, it is evident that the frequency of vibration decreases as the gradient exponent (k) increases. This decrease can be attributed to a reduction in microbeam stiffness as the beam's gradient index increases.

Also, Table 4 and 5 presents the dimensionless natural frequencies using various gradient indexes (k) for (RSGET) and (MCST), considering double-clamped (CC) and clamped-simply (CS) end conditions.

The data in this table highlights how the dimensionless frequency is influenced by the property gradient index (k). The findings suggest that the power index (k) has a contrasting effect on the natural frequencies: an increase in the gradient index leads to a decrease in frequencies, and vice versa. This frequency decrease can be attributed to the changing proportion of ceramic material relative to metal material within the beam as the gradient index rises. Because metal possesses a lower modulus of elasticity compared to ceramics, the beam's flexibility increases, resulting in reduced stiffness and subsequently lower natural frequencies.

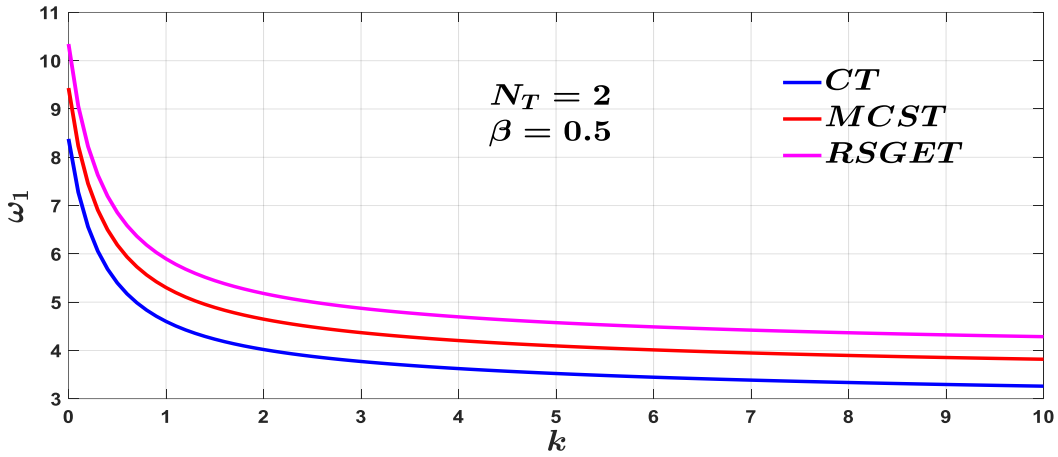

Figure 2 Comparison of 1^{st} order frequency of 2D-FG-microbeam with different theories

Table 4 First four dimensionless natural frequency with CC of different gradient index for L/h = 20, $\beta = 0.5$, $l_m = 17.6\,\mu m$, and $l_s = 0.3\, l_m$

Freq. No.	Thermal Load Factor	MCST				RSGET			
		k							
		0	1	3	5	0	1	3	5
ω_1	$N_T = 0$	24.0640	14.6372	12.4886	11.8718	24.5992	14.9626	12.7639	12.1330
ω_2		66.8654	40.6714	34.7013	32.9875	67.7557	41.2129	35.1567	33.4190
ω_3		131.5267	80.0022	68.2587	64.8877	132.7844	80.7672	68.8985	65.4930
ω_4		217.7587	132.4535	113.0107	107.4295	219.4654	133.4916	113.8751	108.2465
ω_1	$N_T = 2$	23.3965	14.0287	11.9009	11.2875	23.9309	14.3536	12.1755	11.5480
ω_2		65.9700	39.8587	33.9175	32.2088	66.8667	40.4061	34.3785	32.6458
ω_3		130.5512	79.1182	67.4068	64.0415	131.8151	79.8889	68.0519	64.6521
ω_4		216.7370	131.5283	112.1194	106.5443	218.4499	132.5721	112.9890	107.3665

Table 5 First four dimensionless natural frequency with CS of different gradient index for L/h = 20, β = 0.5, $l_m = 17.6\ \mu m$, and $l_s = 0.3\ l_m$

Freq. No.	Thermal Load Factor	MCST				RSGET			
		k							
		0	**1**	**3**	**5**	**0**	**1**	**3**	**5**
ω_1	$N_T = 0$	16.3260	9.9304	8.4727	8.0543	16.5863	10.0887	8.6015	8.1754
ω_2		53.9970	32.8441	28.0229	26.6390	55.1218	33.5283	28.5858	27.1695
ω_3		113.2726	68.8990	58.7853	55.8821	115.5771	70.3007	59.9375	56.9678
ω_4		194.1263	118.0789	100.7461	95.7706	198.0103	120.4414	102.6868	97.5991
ω_1	$N_T = 2$	15.3226	9.0061	7.5760	7.1613	15.5616	9.1447	7.6848	7.2622
ω_2		52.9222	31.8670	27.0802	25.7021	54.0608	32.5639	27.6546	26.2440
ω_3		112.1660	67.8956	57.8182	54.9215	114.4886	69.3138	58.9856	56.0221
ω_4		193.0018	117.0604	99.7648	94.7960	196.9056	119.4408	101.7220	96.6408

Figure 3 illustrates the variation in the fundamental frequency based on (CT), (MCST), and (RSGET) for supported beams with varying thickness gradient indices. The results predicted by the classical theory can be derived from RSGET by setting $l_m = 0$ and $l_s = 0$, while MCST results can be obtained by setting $l_s = 0$. The material-scale parameter of RSGET in this calculation is assumed to be $l_s = 0.3\ l_m$.

As depicted in the Figure 3, the dimensionless first frequency predicted by RSGET and MCST consistently surpasses that obtained from the classical model. This observation also explains the size-dependent behavior. Furthermore, it is evident that the frequency of vibration decreases as the gradient exponent (k) increases. This decrease can be attributed to a reduction in microbeam stiffness as the beam's gradient index increases.

The influence of the composition index (k) on the non-dimensional natural frequencies is presented in Tables 6, 7 and Figures 4 and 5 for C-C and C-S, respectively, with different size scale theories with three axial gradient parameters (β = 0.5, 1, 1.5). The findings indicate that as β increases, the dimensionless frequency decreases.

Furthermore, the results reveal an inverse correlation between the gradient composition index (k) and the dimensionless frequency.

Additionally, the outcomes obtained from the Reformulated Strain Gradient Elasticity (RSGE) theory exhibit higher values compared to those from the Modified Couple Stress (MCS) theory. This difference can be attributed to the higher stiffness predicted by the RSGE theory, resulting in higher frequencies.

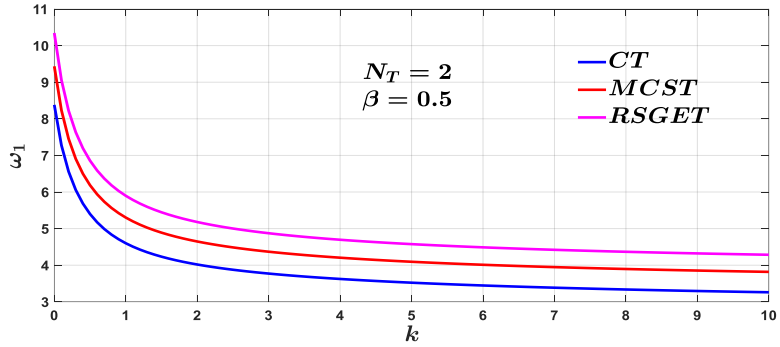

Figure (3): Comparison of 1^{st} order frequency of 2D-FG-microbeam with different theories

Table 6 First order frequency with CC of different gradient index for BDFG microbeams with L/h = 20, $N_T^{\sim} = 2$ and $l_s = 0.3 l_m$, $l_m/h = 0.2$

β	MCST				RSGET			
	k							
	0	**0.5**	**1**	**3**	**0**	**0.5**	**1**	**3**
0	23.9336	16.4487	14.4043	12.2381	24.0547	16.5343	14.4788	12.2994
0.5	23.8087	16.3221	14.2782	12.1134	23.9309	16.4087	14.3536	12.1755
1	23.6664	16.1594	14.1113	11.9433	23.7904	16.2476	14.1883	12.0069

Table 7 First order frequency with CS of different gradient index for BDFG microbeams with L/h = 20, $N_T^{\sim} = 2$ and $l_s = 0.3l_m$, $l_m/h = 0.2$

β	MCST				RSGET			
	k							
	0	**0.5**	**1**	**3**	**0**	**0.5**	**1**	**3**
0	16.1454	11.0076	9.6062	8.1231	16.2306	11.0683	9.6592	8.1669
0.5	15.2267	10.2810	8.9335	7.5090	15.3111	10.3417	8.9868	7.5533
1	14.0217	9.2676	7.9733	6.6060	14.1072	9.3305	8.0290	6.6532

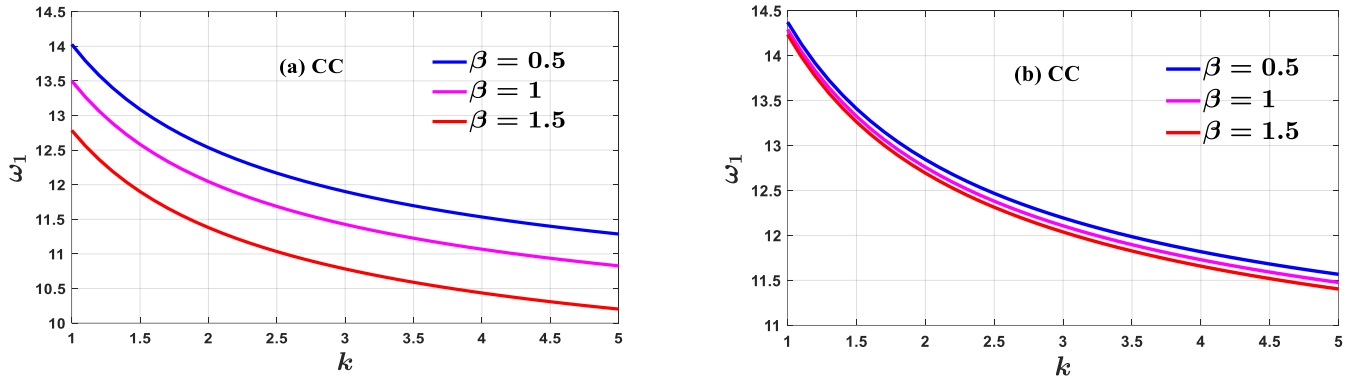

Figure (4): 1^{st} order frequency variation of C-C with various value β based on (a) MCST and (b) RSGET

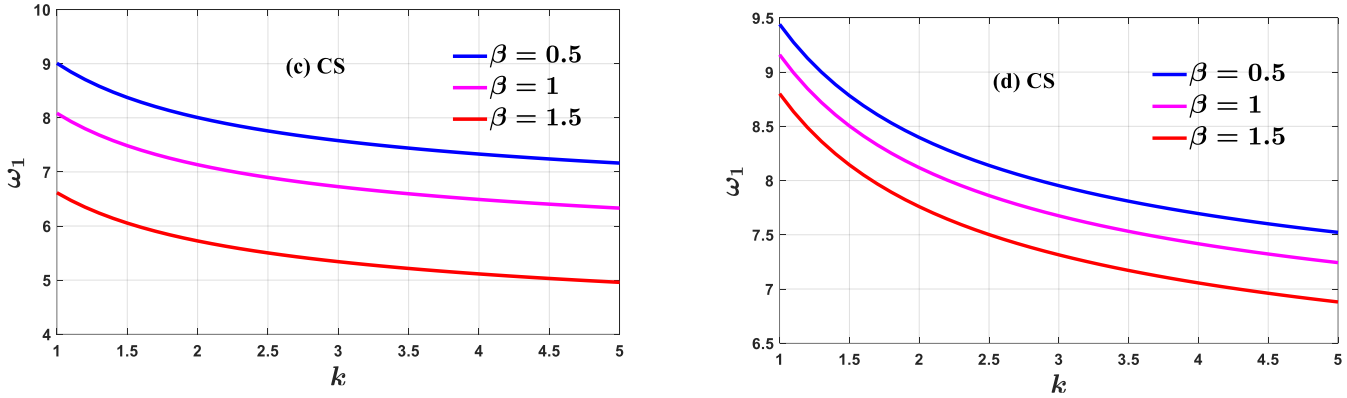

Figure (5): Variation of 1^{st} order frequency of C-S with various value β based on (c) MCST and (d) RSGET

3.2 Influence of Temperature Raise ΔT

Tables 8 and 9 present a visual representation of how temperature increase (ΔT) affects the dimensionless frequencies of the functionally graded (FG) microbeam for both end conditions using here. These tables take into account both the (RSGET) and the (MCST). Utilizing the parameters L/h = 20, $k = 1$, β = 0.5 and $l_m = 17.6\,\mu m$, the calculations reveal that both the Modified Couple Stress Theory (MCST) and the reformulated strain gradient theory (RSGET) exhibit a reduction in dimensionless natural frequencies as the temperature rises.

Additionally, Figures 6 and 7 illustrate the impact of changing temperatures on the system frequency of the functionally graded (FG) microbeam for (C-C) and (C-S) end conditions, respectively. These figures showcase how the system frequency changes at different values of the modified stress length scale ($\boldsymbol{l_m/h}$) and strain length scale ($\boldsymbol{l_s/h}$). The outcomes of the analysis point towards a trend where elevating the length scale ratio parameters leads to higher dimensionless natural frequencies.

Table 8 First four dimensionless natural frequencies with CC of thermal temperature raise for MCST and RSGET of microbeams

Frequency NO.	MCST				RSGET			
	ΔT							
	-80	0	40	80	-80	0	40	80
ω_1	15.6558	14.6372	14.0972	13.5334	15.9836	14.9626	14.4221	13.8583
ω_2	42.0760	40.6714	39.9491	39.2124	42.6082	41.2129	40.4958	39.7648
ω_3	81.5509	80.0022	79.2161	78.4219	82.3062	80.7672	79.9862	79.1973
ω_4	134.0838	132.4535	131.6306	130.8025	135.1123	133.4916	132.6737	131.8507

Table 9 First four dimensionless natural frequencies with CS of thermal temperature raise for MCST and RSGET of microbeams

Frequency NO.	MCST				RSGET			
	ΔT							
	-80	0	40	80	-80	0	40	80
ω_1	11.3719	9.9304	9.1131	8.2050	11.5593	10.0887	9.2540	8.3255
ω_2	34.5125	32.8441	31.9762	31.0836	35.1777	33.5283	32.6716	31.7914
ω_3	70.6486	68.8990	68.0070	67.1029	72.0230	70.3007	69.4233	68.5344
ω_4	119.8696	118.0789	117.1731	116.2601	122.2014	120.4414	119.5515	118.6549

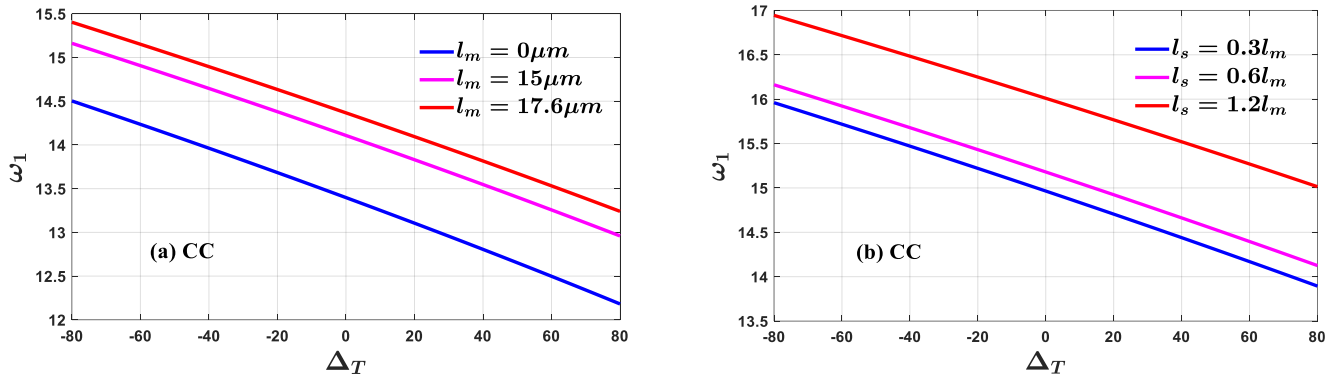

Figure 6 Thermal load effect on 1^{st} order frequency of C-C with various value of l_m and l_s based on (a) MCST and (b) RSGET

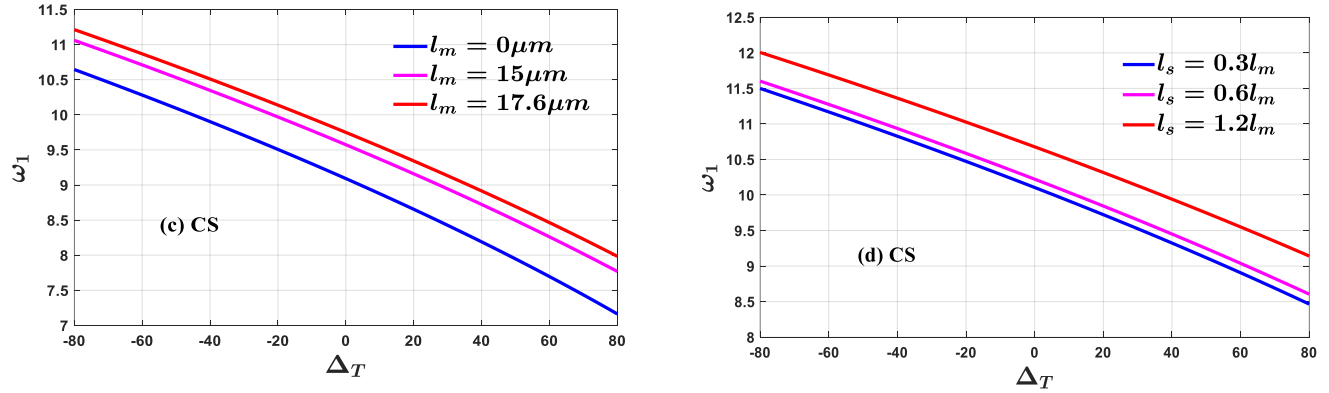

Figure 7 First frequency variation of C-S with various value of l_m and l_s based on (c) MCST and(d) RSGET

4.0 CONCLUSION

The vibrational behavior of a two-dimensional functionally graded (2D-FG) microbeam model was analyzed using the reformulated strain gradient elasticity (RSGE) approach, considering thermal effects. The governing differential equations were derived using the Hamiltonian principle and solved using Galerkin's method (GM) with double-clamped and clamped-simply boundary conditions. The paper focused on investigating the influence of various parameters, including the material gradient index (k), axial gradient index (β), temperature rise (ΔT), and the length scales of couple and strain stress lm and ls, on vibration frequency. The main conclusions of this study:1- Temperature significantly influences the vibrational behavior of 2D-FG microbeams; higher temperatures result in a reduction of the dimensionless natural frequency, 2- The non-dimensional frequencies calculated using the RSGE theory are consistently higher than those obtained from the MCS theory. This disparity can be attributed to the incorporation of two length scales, lm and ls, in the RSGE theory. 3- The natural non-dimensional frequency rises with increasing values of the modified couple (lm) and strain (ls) length scale parameters. Conversely, the frequency decreases with higher values of the axial gradient (β) and material gradation index (k).4- Results obtained under clamped-clamped (c-c) boundary conditions yield larger frequencies compared to those under clamped-simple (c-s) boundary conditions. Additionally, the variations became more pronounced as the beam thickness increased, owing to changes in stiffness based on boundary conditions. 5- The current study's findings align well with previous research, and the tabulated results can serve as a reference for future researchers to validate their findings.

Conflicts of Interest

The author(s) declare(s) that there is no conflict of interest regarding the publication of this paper.

Acknowledgement

The authors express their sincere gratitude to the University of Thi-Qar, Department of Mechanical Engineering for their invaluable support during the completion of this work.

References

[1] Şimşek, M. 2015. Bi-directional Functionally Graded Materials (BDFGMs) for Free and Forced Vibration of Timoshenko Beams with Various Boundary Conditions. *Compos. Struct.* 133: 968-978. Doi: 10.1016/j.compstruct.2015.08.021.

[2] Mohammadi, M., Rajabi, M., and Ghadiri, M. 2021. Functionally Graded Materials (FGMs): A Review of Classifications, Fabrication Methods and Their Applications. *Processing and Application of Ceramics*. 15(4): 319-343. Doi: 10.2298/PAC2104319M.

[3] El-Galy, I. M., Saleh, B. I., and Ahmed, M. H. 2019. Functionally Graded Materials Classifications and Development Trends from Industrial Point of View. *SN Applied Sciences*. 1(11). Doi: 10.1007/s42452-019-1413-4.

[4] Li, X., Li, L., Hu, Y., Ding, Z., and Deng, W. 2017. Bending, Buckling and Vibration of Axially Functionally Graded Beams based on Nonlocal Strain Gradient Theory. *Compos. Struct.* 165: 250-265. Doi: 10.1016/j.compstruct.2017.01.032.

[5] Tang, Y., Lv, X., and Yang, T. 2019. Bi-directional Functionally Graded Beams: Asymmetric Modes and Nonlinear Free Vibration. *Compos. Part B Eng.* 156: 319-331. Doi: 10.1016/j.compositesb.2018.08.140.

[6] Elaikh, T. E., Abed, N. M. 2019. Stability of FG Material Micro-pipe Conveying Fluid. *International Journal of Energy and Environment*. 10(4): 211-222.

[7] Ghayesh, M. H., and Farokhi, H. 2016. Coupled Nonlinear Dynamics of Geometrically Imperfect Shear Deformable Extensible Microbeams. *J. Comput. Nonlinear Dyn.* Doi: 10.1115/1.4031288.

[8] Ghayesh, M. H., and Farajpour, A. 2019. A Review on the Mechanics of Functionally Graded Nanoscale and Microscale Structures. *Int. J. Eng. Sci.* 137: 8-36. Doi: 10.1016/j.ijengsci.2018.12.001.

[9] Elaikh, T. E. H., Abed, N. M., and Ebrahimi-Mamaghani, A. 2020. Free Vibration and Flutter Stability of Interconnected Double Graded Micro Pipes System Conveying Fluid. *IOP Conf. Ser. Mater. Sci. Eng.* Doi: 10.1088/1757-899X/928/2/022128.

[10] Şimşek, M. 2016. Buckling of Timoshenko Beams Composed of Two-Dimensional Functionally Graded Material (2D-FGM) Having Different Boundary Conditions. *Compos. Struct.* Doi: 10.1016/j.compstruct.2016.04.034.

[11] Avcar, M. 2014. Free Vibration Analysis of Beams Considering Different Geometric Characteristics and Boundary Conditions. *Int. J. Mech. Appl.* 4(3): 94-100. Doi: 10.5923/j.mechanics.20140403.03.

[12] Karamanli, A., and Thuc, P. Vo. 2020. Bending, Vibration, Buckling Analysis of bi-directional FG Porous Microbeams with a Variable Material Length Scale Parameter. *Appl. Math. Model.* Doi: 10.1016/j.apm.2020.09.058.

[13] Şimşek, M. 2010. Dynamic Analysis of an Embedded Microbeam Carrying a Moving Microparticle based on the Modified Couple Stress Theory. *Int. J. Eng. Sci.* 48(12): 1721--1732. Doi: 10.1016/j.ijengsci.2010.09.027.

[14] Asghari, M., Ahmadian, M. T., Kahrobaiyan, M. H. and Rahaeifard, M. 2010. On the Size-dependent Behavior of Functionally Graded Micro-beams. *Mater. Des.* 31(5): 2324-2329. Doi: 10.1016/j.matdes.2009.12.006.

[15] Liu, H., and Zhang, Q. 2021. Nonlinear Dynamics of Two-directional Functionally Graded Microbeam with Geometrical Imperfection using Unified Shear Deformable Beam Theory. *Appl. Math. Model.* 98: 783-800. Doi: 10.1016/j.apm.2021.05.029.

[16] Lam, D. C. C., Yang, F., Chong, A. C. M., Wang, J., and Tong, P. 2003. Experiments and Theory in strain Gradient Elasticity. *J. Mech. Phys. Solids*. 51(8): 1477-1508. Doi: 10.1016/S0022-5096(03)00053-X.

[17] Akgöz, B., and Civalek, Ö. 2013. Buckling Analysis of Functionally Graded Microbeams based on the Strain Gradient Theory. *Acta Mech.* 224(9): 2185-2201. Doi: 10.1007/s00707-013-0883-5.

[18] Ansari, R., Gholami, R., and Sahmani, S. 2014. Free Vibration of Size-dependent Functionally Graded Microbeams based on the Strain Gradient Reddy Beam Theory. *Int. J. Comput. Methods Eng. Sci. Mech.* 15(5): 401-412. Doi: 10.1080/15502287.2014.915249.

[19] Attia, M. A., and Shanab, R. A. 2022. On the Dynamic Response of bi-directional Functionally Graded

Nanobeams under Moving Harmonic Load Accounting for Surface Effect. *Acta Mech.* 233(8): 3291-3317. Doi: 10.1007/s00707-022-03243-1.

[20] Chen, L., Liu, Y., Zhou, S., and Wang, B. 2021x. The Reformulated Micro-beam Models by Incorporating the General Strain Gradient Elasticity Theory (GSGET). *Appl. Math. Model.* 90: 448-465. Doi: 10.1016/j.apm.2020.08.050.

[21] Yin, S., Xiao, Z., Liu, J., Xia, Z., and Gu, S. 2022. Variational Formulations and Isogeometric Analysis of Timoshenko–Ehrenfest Microbeam Using a Reformulated Strain Gradient Elasticity Theory. *Crystals*. 12(6). Doi: 10.3390/cryst12060752.

[22] Dinachandra, M., and Alankar, A. 2021. Static and Dynamic Modeling of functionally Graded Euler–Bernoulli Microbeams based on Reformulated Strain Gradient Elasticity Theory using Isogeometric Analysis. *Compos. Struct.* 280: 114923. Doi: 10.1016/j.compstruct.2021.114923.

[23] Yin, S., Xiao, Z., Zhang, G., Bui, T. Q., Wang, X., and Liu, J. 2022. Size-dependent Postbuckling for Microbeams: Analytical Solutions using a Reformulated Strain Gradient Elasticity Theory. *Acta Mech.* 233(12): 5045-5060. Doi: 10.1007/s00707-022-03360-x.

[24] Yin, S., Xiao, Z., Zhang, G., Liu, J., and Gu, S. 2022. Size-Dependent Buckling Analysis of Microbeams by an Analytical Solution and Isogeometric Analysis. *Crystals*. Doi: 10.3390/cryst12091282.

[25] Yin, S., Xiao, Z., Deng, Y., Zhang, G., Liu, J., and Gu, S. 2021. Isogeometric Analysis of Size-dependent Bernoulli–Euler Beam based on a Reformulated Strain Gradient Elasticity Theory. *Comput. Struct.* 253: 106577. Doi: 10.1016/j.compstruc.2021.106577.

[26] Zhang, G. Y., and Gao, X. L. 2020. A New Bernoulli–Euler Beam Model based on a reformulated Strain Gradient Elasticity Theory. *Math. Mech. Solids*. 25(3): 630-643. Doi: 10.1177/1081286519886003.

[27] Babaei, A., Noorani, M. R. S., and Ghanbari, A. 2017. Temperature-dependent Free Vibration Analysis of Functionally Graded Micro-beams based on the Modified Couple Stress Theory. *Microsyst. Technol.* 23(10): 4599-4610. Doi: 10.1007/s00542-017-3285-0.

[28] Zanoosi, A. A. P. 2020. Size-dependent Thermo-mechanical Free Vibration Analysis of Functionally Graded Porous Microbeams based on Modified Strain Gradient Theory. *J. Brazilian Soc. Mech. Sci. Eng.* 42(5). Doi: 10.1007/s40430-020-02340-3.

[29] Tang, Y., and Ding, Q. 2019. Nonlinear Vibration Analysis of a bi-directional Functionally Graded Beam under Hygro-thermal Loads. *Compos. Struct.* 111076. Doi: 10.1016/j.compstruct.2019.111076.

[30] Nateghi, A., and Salamat-talab, M. 2013. Thermal Effect on Size Dependent Behavior of Functionally Graded Microbeams based on Modified Couple Stress Theory. *Compos. Struct.* 96: 97-110. Doi: 10.1016/j.compstruct.2012.08.048.

[31] Liu, H., Zhang, Q., and Ma, J. 2021. Thermo-mechanical Dynamics of Two-dimensional FG Microbeam Subjected to a Moving Harmonic Load. *Acta Astronaut.* 178(January): 681-692. Doi: 10.1016/j.actaastro.2020.09.045.

[32] Tang, Y., Zhong, S., Yang, T., and Ding, Q. 2019. Interaction between Thermal Field and Two-dimensional Functionally Graded Materials: A Structural Mechanical Example. *Int. J. Appl. Mech.* 11(10). Doi: 10.1142/S1758825119500996.

[33] Ebrahimi-Mamaghani, A., Sotudeh-Gharebagh, R., Zarghami, R., and Mostoufi, N. 2020. Thermo-mechanical Stability of Axially Graded Rayleigh Pipes. *Mech. Based Des. Struct. Mach*. 1-30. Doi: 10.1080/15397734.2020.1717967.

[34] Elaikh, T. E., and Agboola, O. O. O. 2022. Investigation of Transverse Vibration Characteristics of Cracked Axially Moving Functionally Graded Beam Under Thermal Load. *Trends Sci.* 19(23). Doi: 10.48048/tis.2022.1349.

[35] Mutlak, D. A., Muhsen, S., Waleed, I., Hadrawi, S. K., Khaddour, M. H., and Ahmadi, S. 2022. Forced and Free Dynamic Responses of Functionally Graded Porous Rayleigh Small-Scale Beams on Kerr Foundation under Moving Force. *Mater. Today Commun.* 33: 104919. Doi: 10.1016/J.MTCOMM.2022.104919.

[36] Nematollahi, M. S., Mohammadi, H., and Taghvaei, S. 2019. Fluttering and Divergence Instability of Functionally Graded Viscoelastic Nanotubes Conveying Fluid based on Nonlocal Strain Gradient Theory. *Chaos*. 29(3). Doi: 10.1063/1.5057738.

[37] Nejad, M. Z., and Hadi, A. 2016. Non-local Analysis of Free Vibration of bi-directional Functionally Graded Euler-Bernoulli Nano-beams. *Int. J. Eng. Sci.* 105: 1-11. Doi: 10.1016/j.ijengsci.2016.04.011.

[38] Yapor Genao, F., Kim, J., and Żur, K. K. 2021. Nonlinear Finite Element Analysis of Temperature-dependent Functionally Graded Porous Micro-plates under Thermal and Mechanical Loads. *Compos. Struct.* 256: 112931. Doi: 10.1016/j.compstruct.2020.112931.

[39] Esen, I., Özarpa, C., and Eltaher, M. A. 2021. Free Vibration of a Cracked FG Microbeam Embedded in an Elastic Matrix and Exposed to Magnetic Field in a Thermal Environment. *Compos. Struct.* 261x. Doi: 10.1016/j.compstruct.2021.113552.

[40] Shaat, M. 2018. A reduced Micromorphic Model for Multiscale Materials and Its Applications in Wave Propagation. *Compos. Struct.* 201: 446-454. Doi: 10.1016/j.compstruct.2018.06.057.

[41] Zhang, G. Y., Gao, X. L., Zheng, C. Y., and Mi, C. W. 2021. A Non-classical Bernoulli-Euler Beam Model based on a Simplified Micromorphic Elasticity Theory. *Mech. Mater.* 161: 103967. Doi: 10.1016/j.mechmat.2021.103967.

[42] Rao, S. S. 2007. *Vibration of Continuous Systems.* Doi: 10.1002/9780470117866.

[43] Eltaher, M. A., Emam, S. A., and Mahmoud, F. F. 2012. Free Vibration Analysis of Functionally Graded Size-dependent Nanobeams. *Appl. Math. Comput.* 218(14): 7406-7420. Doi: 10.1016/j.amc.2011.12.090.